Electric Double Layer at the Rutile (110) Surface. 3. Inhomogeneous Viscosity and Diffusivity Measurement by Computer Simulations

ARTICLE *in* THE JOURNAL OF PHYSICAL CHEMISTRY C · FEBRUARY 2007

Impact Factor: 4.77 · DOI: 10.1021/jp065165u

Electric Double Layer at the Rutile (110) Surface. 3. Inhomogeneous Viscosity and Diffusivity Measurement by Computer Simulations

M. Předota,*,†,‡ P. T. Cummings,§,|| and D. J. Wesolowski||

Department of Medical Physics and Biophysics, University of South Bohemia, Jírovcova 24, České Budějovice 370 04, Czech Republic, Institute of Chemical Process Fundamentals, Academy of Sciences of the Czech Republic, 165 02 Prague, Czech Republic, Department of Chemical Engineering, Vanderbilt University, Nashville, Tennessee 37235-1604, and Aqueous Chemistry and Geochemistry Group, Chemical Sciences Division, Oak Ridge National Laboratory, Oak Ridge, Tennessee 37831-6110

Received: August 10, 2006; In Final Form: November 7, 2006

Molecular dynamics simulations were conducted to characterize the dynamic properties of the interface between aqueous electrolyte and the (110) surface of rutile (α-TiO_2). For the first time, the inhomogeneous viscosity of water (at liquid density) in a slab formed by two rutile surfaces was determined computationally. The viscosity and diffusivity profiles show three different regions as a function of distance from the surface: (i) a region of two adsorbed layers of water molecules with apparently infinite viscosity and zero diffusivity, (ii) an interfacial inhomogeneous region consisting of additional 2−3 layers, and (iii) bulk-liquid behavior recovered as close as 15 Å from the surface. The second layer of adsorbed water molecules becomes more loosely bound to the surface with increasing temperature up to 523 K. Our results supplement our previous structural findings and confirm that not only the structural but also the dynamic properties of the interface indicate that bulk properties are recovered within about 15−20 Å from the surface.

1. Introduction

In our previous papers,[1−3] we described the modeling of rutile (α-TiO_2) surfaces in contact with aqueous solution and presented results on the structure of water and ions at the interface. Our molecular dynamics simulation results agree very well with experimental data obtained by X-ray standing wave (XSW) and X-ray reflectivity (e.g., crystal truncation rod (CTR)) analysis of surface structures,[4,5] which can be treated as validation of our model and enables us to extend the range of investigated properties to dynamic properties of the aqueous solution in contact with the rutile surface.

Our main goal of this paper is the determination of space-dependent viscosity of water in contact with the rutile (110) surface. Our results (i) extend the application of a methodology for determination of space-dependent viscosity to a more complex system, (ii) give information on the dynamic properties of water in contact with the rutile surface, and (iii) enable us to discuss possible sources of discrepancy between our results[1−5] and results of electrophoretic measurements.

Unlike the determination of structural properties at the interface, the determination of dynamic properties by molecular simulation is scarce. The determination of space-dependent viscosity has been implemented mostly for atomic fluids based on the Lennard-Jones potential or its modifications,[6−10] and studies for molecular fluids, namely water, are rare.[11,12] A recent paper by Freund[11] discussed the dynamic properties of SPC/E water containing Cl^- ions adjacent to a smooth, positively charged wall of generic Lennard-Jones atoms. In this paper, we explore the dynamic interaction of SPC/E water with the atomistically detailed rutile (110) surface.[1,2] Since the viscosity is measured in a slab system subject to a shear generated by external applied force, proper thermostatting was an important issue. In addition to viscosity measurement from nonequilibrium molecular dynamics, we determined local, inhomogeneous diffusivity of water at the rutile interface from equilibrium molecular dynamics by tracking the mean square displacement of water molecules separated into bins parallel with the interface.

2. Model

Water is modeled using the SPC/E model[13] and the surface model of rutile is based on ab initio obtained[1,14,15] potentials and structure. The bare rutile (110) surface is characterized by a plane of Ti atoms, including rows of bare, five-coordinated Ti atoms and six-coordinated Ti atoms bonded to rows of doubly coordinated bridging oxygens (BO) that protrude above the Ti plane. The Ti surface plane also includes rows of triply coordinated oxygens. The bare terminal Ti atoms are always covered by either a strongly associated water molecule (non-hydroxylated surface) or a bonded hydroxyl group referred to as the terminal hydroxyl; the oxygen of the hydroxyl group becomes terminal oxygen (TO), singly coordinated with originally five-coordinated Ti atom (hydroxylated surface). In our simulations, the bond lengths of the BO and TO with surface titanium atoms are fixed at their ab initio values, but the bonds are permitted to wag. All atoms on and below the surface plane are relaxed to their ab initio configuration but are held rigid in the simulations, since their motion is restricted to thermal vibrations within less than 0.1 Å, and are therefore of little influence on the interfacial structure. This is particularly true for the properties studied here. For the potential parameters and figures of the structure, the reader is referred to the previous papers of this series.[1,2]

The molecular dynamics simulations of TiO_2−water interfaces were performed in slab geometry with aqueous solutions

† University of South Bohemia.
‡ Academy of Sciences of the Czech Republic.
§ Vanderbilt University.
|| Oak Ridge National Laboratory.

10.1021/jp065165u CCC: $37.00
Published on Web 01/31/2007

TABLE 1: Parameters of Our Simulations: Temperature T, Bulk Density ρ_{bulk}, Resulting Pressure P, Half of the Slab Width L_z; and the Experimental Values of Viscosity, η, Diffusivity, D, and Pressure P_{exp}

			narrow slab	wide slab			
T [K]	ρ_{bulk} [g/cm^3]	P [bar]	$L_z/2$	$L_z/2$	η [10^{-4} Pa.s]	D [10^{-9} m^2/s]	P_{exp} [bar]
298	1.00	3 ± 6	23.3	44.3	8.90 [ref 27]	2.3 [refs 29, 30] SPC/E 2.7 [ref 28]	1.0
448	0.89	60 ± 6	26.0	49.4	1.55 [ref 27]	19.6 [ref 31]	8.9 [ref 27]
523	0.79	233 ± 6	28.7	54.6	1.06 [ref 27]	31.7 [ref 30]	39.7 [ref 27]

sandwiched between two parallel TiO_2 (110) walls (see Figure 3 of ref 1). Therefore, the system has two identical solid−fluid interfaces. The whole system is periodically replicated in the lateral x and y directions parallel to the surface plane.

In this paper, we report results of the dynamic properties of pure water between two neutral (zero charged) (110) rutile surfaces only. It would be of even higher relevance to determine the dynamic properties at negative surfaces under close to real conditions, as in our previous studies. However, the determination of local viscosity is a new topic and so far was applied only to pure fluids; that is, the generalization of this approach to mixtures is not theoretically developed yet, and we are therefore restricted to study a pure fluid−water. There are however important facts, which justify us to believe that results obtained for the simplified system adopted here (i.e., no surface charge and no dissolved ions) are characteristic even for the negatively charged system observed under experimental conditions. These are namely little effect of surface charge and presence of ions on (i) the structure of water (Figures 4 and 5 of ref 1), (ii) the axial profiles of electrostatic properties (Figure 7 of ref 1), and (iii) the diffusivity of water at 298 and 448 K outside of the layer of adsorbed ions (Figure 9 of ref 1).

The technical details of our simulations are the same as in our previous simulations[1,2] unless specified otherwise. The simulation length was about 2 ns. For each temperature, we first adjust the separation of the two surfaces to yield density in the center of the slab equal to experimental bulk density at the same temperature. The resulting pressure, which was found to be independent of the applied external force, results from the thermodynamics of the model and at high temperatures exceeds the experimental pressure at a given temperature and density, see Table 1. We decided to set the density in the bulk, since that is a property, which can be accurately measured, whereas pressure, calculated from the force exerted on the walls, is subject to significant inaccuracy (of the order of 10 bar). Running the NVT simulations also has some minor technical advantages (since we register the properties in narrow bins, it is convenient to keep the number and width of these bins constant).

3. Local Viscosity Determination

The main motivation for our study of local viscosity in the slab was a remarkable disagreement between the structural results of our molecular dynamics (MD) simulations and X-ray structural measurements on one hand and, on the other hand, current theories for interpreting electrokinetic measurements at oxide/water interfaces in terms of a "shear plane" at a considerable distance from the surface, which is strongly dependent on the solution ionic strength, becoming greater with decreasing ionic strength. The MD and X-ray results[5] both agree that the influence of the surface on the aqueous solution reaches no more than 15−20 Å from the rutile surface, whereas the so-called "shear plane", based on interpretation of the electrophoretic data, is inferred to be about 80 Å from the rutile surface in 0.001 m electrolyte solution.[16] Evidently, this value is based on a simplified picture of the interface, splitting the continuously varying interface into a region of ions and water molecules which move with the particle (immobile layer), and the diffuse layer followed by a bulk fluid, with a specific, but ill-defined "shear" plane separating the immobile and diffuse layers. However, this cannot be fully responsible for the significant discrepancy observed, which lead us to investigate the approximations behind the interpretation of electrophoretic data in more detail and particularly, to computationally determine the inhomogeneous viscosity profile of water in the rutile−water slab. In electrophoretic measurements, the directly measured property is the mobility of charged particles in the external electric field.[17] The velocity of the particles is recorded, and from the observed distance, time, and electric field, the mobility can be directly and accurately determined. One of the key properties determined by the experimentalists is the zeta potential at the shear plane ζ, which is usually calculated using the Helmholtz−Smoluchowski equation

$$\zeta = \frac{\eta}{\epsilon_0 \epsilon_r} \mu$$

where η is the solvent shear viscosity, ϵ_0 is the permittivity of vacuum, ϵ_r is the relative permittivity (dielectric constant) of the solvent, and μ is the observed mobility of the particles. However, it is well-known, that the permittivity changes dramatically in the interface, with values going from the bulk value of about 80 at room temperature to as low as 6−20 at the contact layer,[18] though the concept of the dielectric constant may not be adequately defined for molecular fluids at distances of a few molecular diameters, particularly at interfacial boundaries, where the bulk fluid structure is highly disrupted. Similarly, one must expect that the viscosity in the inhomogeneous region, where density varies by a factor of 3, might significantly vary from its bulk value. The steep increase of viscosity of water in contact with a surface has already been observed by computer simulations.[11] However, none of these aspects is taken into account in the Helmholtz−Smoluchowski equation, mostly because of the lack of the detailed, space-dependent variations of the permittivity and viscosity. Nevertheless, there are electrokinetic studies [e.g., ref 19], which find experimental electrokinetic data, interpreted with the Helmholtz−Smoluchowski equation, best fitted with a slip plane at only about 15 Å from the rutile surface.

There are two main approaches to determine shear viscosity of a fluid from molecular dynamics simulations namely equilibrium or nonequilibrium simulations. The equilibrium approach[20−21] is based on the determination of the viscosity from the fluctuations of off-diagonal components of pressure tensor or integration of corresponding autocorrelation function.[22,23] Due to the fact that the off-diagonal pressure component in these formulas is given by the sum over all molecules of the system and cannot be easily split into single molecule properties (as, e.g., in diffusivity calculations), this approach seems impossible to apply unless a proper theoretical base is developed. We therefore applied nonequilibrium molecular dynamics[6,11,24] to

determine the viscosity from the fluid subject to the external force along the surface. Denoting the lateral dimensions of the surface as x and y, and as z the normal direction to the surface, water was subject to a constant force F_x acting on the center of mass of each water molecule. As a result, a velocity profile $\langle v_x(z)\rangle$ develops, corresponding to a Poiseuille flow. From this velocity profile, we were able to derive the local viscosity as described below.

In an idealization of a homogeneous fluid between two wetting walls, the velocity profile is parabolic

$$v_x(z) = \frac{\rho F_x}{2\eta}\left(\frac{L_z^2}{4} - z^2\right)$$

where ρ is the assumed constant density, η is the assumed constant shear viscosity, L_z is the surface to surface distance, and z is the axial coordinate, $-L_z/2 < z < L_z/2$. In reality, the observed velocity profile is not exactly parabolic, but one can define local shear rate as $\gamma(z) = \mathrm{d}v_x(z)/\mathrm{d}z$, where the derivative is carried out either by direct numerical derivative of the velocity profile $v_x(z)$ or by fitting a polynomial to the velocity profile and taking the derivative algebraically. The local viscosity is related to the local shear rate via

$$\eta(z) = -\lim_{F_x \to 0} \frac{\langle P_{xz}(z)\rangle}{\gamma(z)}$$

where $\langle P_{xz}(z)\rangle$ is the average value of the off-diagonal component of the pressure tensor.[6] Unlike homogeneous simulations, the slab geometry offers a surprisingly easy and straightforward way to calculate the average of this component, as derived in refs 7 and 25. According to this study, the $\langle P_{xz}(z)\rangle$ component can be obtained via integration of the easily accessible density profile of water molecules, $P_{xz}(z) = F_x \int_0^z \rho(z')\,\mathrm{d}z'$, where z is the axial coordinate and $z = 0$ giving the center of the slab.

The fully atomistic rutile surface reveals different structure along the x coordinate (lines of alternating bridging and terminal sites, spacing 6.5 Å) and y coordinate (lines of sites of the same kind, spacing 2.96 Å). Therefore, in selected simulations, we have applied the force either in x or y directions to find out if the direction of applied force relative to surface structure plays a role. Since that was not observed, all presented results are for external force F_x.

4. Thermostatting of the System

Since the external applied force exerts work on the system and heats it, it is essential to remove this extra generated heat by a proper thermostat. Most of the simple thermostats originate from the calculation of root-mean-square velocity, from which the translational kinetic temperature is calculated as $T_{\mathrm{kin}} \sum_{i=1}^{N} m_i \mathbf{v}_i^2/fk_{\mathrm{B}}$, where m_i is the mass of molecule i, f is the number of translational degrees of freedom ($f = 3N - 3$, where N is the number of molecules), and k_{B} is Boltzmann's constant. If one wishes to apply this definition of kinetic temperature to a system under flow, it is essential to subtract the nonzero streaming velocity in the direction of the flow, though sometimes small streaming velocity is ignored.[11,12] If the external force along the x direction is applied, one needs to calculate the translational kinetic energy K as $K = 1/2\sum_{i=1}^{N} m_i[(v_{xi} - \bar{v}_x(z_i))^2 + v_{y_i}^2 + v_{zi}^2]$, where $\bar{v}_x(z_i)$ is the average streaming velocity in the layer given by the z coordinate of the molecule. This approach suffers from several drawbacks: (i) the average velocity profile must be known prior to production runs and can be obtained only from the simulations, i.e., one has to iterate the velocity profile, using an improved value for more accurate thermostatting of the system; (ii) for molecular fluids, the stream leads to "rolling" of the molecules along the surface, contributing to transfer of energy between the translational and rotational degrees of freedom.

Therefore, we decided to apply a simpler thermostat as follows. The design of this thermostat stems from the identification of three different roles of system coordinates. The z coordinate runs perpendicular to the surface and thus all properties vary along this coordinate as a result of the inhomogeneity. The x coordinate is the coordinate of the applied external force. Excluding the inhomogeneity induced by the surface structure, the system is homogeneous in this direction, but the distribution of velocity v_x is complex due to the external force. The y direction is homogeneous (excluding the inhomogeneity induced by the surface structure) and the distribution of velocity v_y is given by the Maxwell−Boltzmann distribution. We therefore calculate the kinetic temperature only based on the values of v_y, i.e., $T_{\mathrm{kin}} = \sum_{i=1}^{N} m_i v_{y_i}^2/((N-1)k_{\mathrm{B}})$, where the number of degrees of freedom $N - 1$ is considered, taking into account N molecules and conservation of the p_y momentum component. No thermostatting of the other components of translational velocity or any of the rotational components of velocity is applied. The thermostatting of these velocities is provided only via redistribution of the energy among all degrees of freedom. The thermostatting of only the perpendicular component of velocity relative to flow direction given by external force proved in a study of atomic fluid[8] to be superior to thermostatting any other velocity components and the closest in performance to that of configurational thermostat.[8,26] Thermostatting of both velocity components perpendicular to the applied field has been used in a study of atomic fluid.[9,10]

5. Results

We have performed simulations at ambient conditions $T =$ 298 K, $\rho_{\mathrm{bulk}} = 1$ g/cm^3 (the density of liquid water at 1 atm and 298 K), and at two high-temperature states $T = 448$ and 523 K with bulk density chosen to equal to the density of liquid water in equilibrium with its vapor at each temperature;[27] see Table 1. We used two system sizes to verify that our results are not size-dependent. A system with 2048 water molecules has surface dimensions $L_x = 39.0$ Å and $L_y = 35.5$ Å, i.e., 6 times the lattice spacing $c_x = 6.50$ Å and 12 times the lattice spacing $c_y = 2.96$ Å. The width of the slab was adjusted in each case to yield the desired bulk density in the center and was about 50 Å. A system with 1728 water molecules has surface dimensions $L_x = 26.0$ Å and $L_y = 23.7$ Å, i.e., 4 times the lattice spacing c_x and 8 times the lattice spacing c_y. The resulting width of the slab is about twice than in the former system, therefore, we identify them as wide and narrow slabs, respectively. However, the identification "narrow" has only relative meaning, homogeneous bulk phase is well developed in both systems and no interference of the two parallel surfaces is observed in any case.

Viscosity. The external force F_x must be large enough to enable determination of the streaming velocity profile $\bar{v}_x(z)$ from the background thermal noise. Considering that the root-mean-square velocity corresponding to 298 K is 371 m/s, it is evident that one needs the streaming velocity to be of the order of tens of m/s. At the same time, one needs the external force F_x to be small enough to be in the linear flow regime and to minimize the amount of heat generated. By a method of trial and error, we found that a very good compromise is to choose F_x equal to 3.4×10^{-13} N. For comparison, this is the magnitude of the

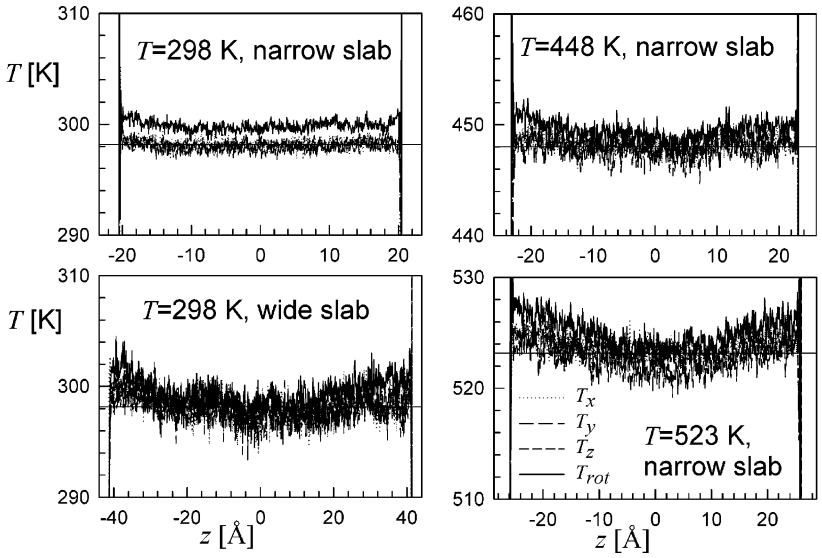

Figure 1. Kinetic temperatures of all three components of translational velocity with average streaming velocity $v_x(z)$ subtracted and rotational temperature. The kinetic temperature of each component is proportional to the root-mean-square velocity. The temperature of the thermostat is indicated by horizontal line.

Lennard-Jones attraction between two oxygen atoms in two SPC/E water molecules at distance 6.91 Å, i.e., $2.2\sigma_{SPC/E}$, where $\sigma_{SPC/E}$ is the Lennard-Jones size parameter of this interaction. For higher temperatures and wide slab, the external force can be reduced by a factor 3−10 and still give good statistics of the streaming velocity.

In Figure 1, we give the temperature profile of all three translational components of kinetic temperature, with the mean streaming velocity $\bar{v}_x(z)$ subtracted, and rotational component of kinetic temperature to demonstrate the performance of the applied thermostat. Except the simulation at ambient conditions in a narrow slab, the temperature profile is slightly parabolic with elevated temperature closer to the surfaces and reduced temperature in the center. The first feature is linked to the shear stress and shear rate profile, which grows approximately linearly with increasing distance from the center; that is, the generation of heat is largest at layers furthest from the center. The second feature is caused by thermostatting based on summed kinetic energy of all water molecules. The profile of all three translational components of kinetic temperature is the same and fluctuates around the preset temperature, though only the *y*-component of velocity is subject to thermostatting; this proves that the energy transfer among translational degrees of freedom is efficient. The rotational component of kinetic temperature is always slightly higher than the preset temperature, typically by 2−3 K. This fact, together with the slightly parabolic profile of temperatures, shows limitations of the applied thermostat. However, we argue that (i) the performance of the applied thermostat is sufficient for the purpose of this paper, i.e., presentation of the methods and results relevant for ongoing interpretation of experimental results for rutile/aqueous solution interface, and (ii) the only realistic thermostat is a thermostat which removes the heat only via the slab walls and not water molecules directly, a situation leading to development of a complex temperature profile.

The velocity profile at ambient conditions is shown in Figure 2 for a narrow slab. Prior to analyzing the velocity and viscosity profiles, the detailed description of the properties of the interfacial region in the closest vicinity of the surface, shown in Figure 3 for both hydroxylated (top) and nonhydroxylated (bottom) surfaces, must be discussed. The hydroxylated rutile surface is terminated by rows of terminal hydroxyls at 2 Å, indicated in the density plot in Figure 3. No water molecules penetrate closer to the surface than 2.9 Å and the peak at 3.7 Å is the position of a layer of physisorbed water molecules which occupy well-defined sorption sites relative to the 110 surface.[1] Because of low density, the velocity profile at distances just above 2.9 Å suffers from huge numerical uncertainties, and therefore, only the distances larger than 3.3 Å were considered for viscosity determination. At the nonhydroxylated surface (Figure 3, bottom), there is a layer of water molecules physisorbed above terminal Ti atoms at 2.3 Å from the surface and an additional layer of physisorbed water molecules at 3.7 Å, just as in the case of hydroxylated surface. In the physisorbed layer at 2.3 Å, the streaming velocity is zero, indicating that these molecules stay adsorbed to their sites throughout the time scale of the simulation. Once again, the velocity profile at distances between 2.6 and 3.3 Å suffers from inaccuracy due to density of water approaching zero and, as for the hydroxylated surface, only the distances larger than 3.3 Å were considered for viscosity determination. We can conclude the comparison of the two surfaces by a statement that already the second layer of water is quite similar for both hydroxylated and nonhydroxylated surfaces. The results presented are for the hydroxylated surface, which has been recognized to more closely mimic the real rutile surface,[2,5] but we always checked that the results for the nonhydroxylated surface show the same features.

The velocity profile (Figure 2a) is close to parabolic; however, in the vicinity of the surfaces, the slope of the velocity profile as a function of distance from the surface approaches zero, as the velocity profile itself approaches zero. This is caused by a strong adsorption of not only the first but also the second layer of water molecules[1] preventing them from leaving their adsorption sites. Since these adsorbed water molecules are subject to the external force as any other water molecule, we can immediately see that these molecules will exhibit extremely large (theoretically diverging to infinity) viscosity, since shear viscosity can be interpreted as reluctance of a molecule to undergo shear when exposed to an external force. This result is distinctly different from simulation of SPC/E water in contact with a smooth wall of generic Lennard-Jones atoms,[11] in which case the viscosity in contact layer was found to increase by a

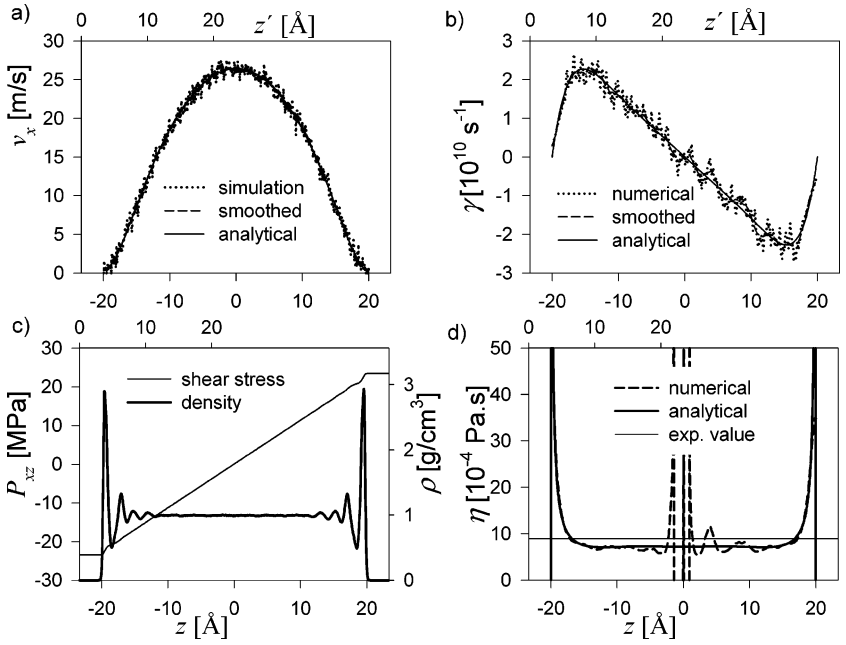

Figure 2. Velocity profile (a), shear rate (b), shear stress and density profile (c), and resulting viscosity profile (d) at ambient conditions, narrow slab. The experimental value of viscosity at 298 K is $\eta = 8.9 \times 10^{-4}$ Pa.s.[27] The z-coordinate is centered in the middle of the slab. The coordinate $z' = L_z/2 - z$, which gives the distance from a surface, is given on top of graphs.

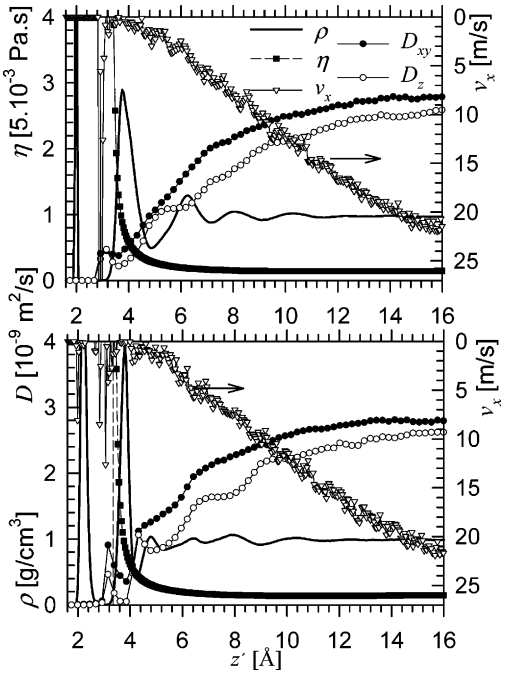

Figure 3. Detailed view of the properties of interfacial region for hydroxylated (top) and nonhydroxylated (bottom) surface at ambient conditions. The values of density ρ, parallel and perpendicular diffusivities D_{xy} and D_z, and numerically obtained viscosity η are shown in corresponding units on the left axis. The streaming velocity profile v_x is given by the right axis, which is inversed to avoid overlapping of the curves.

factor of 6, relative to bulk water, but not to approach infinity, since the contact layer was not completely immobile.

We have applied two methods to determine the shear rate and resulting viscosity profile. One approach starts with approximation of the velocity profile with a polynomial and carrying out subsequent algebraic manipulations with this fitted dependence. Since the profile is symmetric with respect to z coordinate, we adopted the form $v_x(z) = a_0 + a_2z^2 + a_4z^4 + a_6z^6 + a_8z^8$. The number of terms considered slightly affects the resulting curves, particularly at the center of the slab, but our findings are fit independent as long as at least constant, quadratic, and quartic terms are included. Having the velocity profile fitted, the shear rate is obtained as $\gamma(z) = dv_x(z)/dz = 2a_2z + 4a_4z^3 + 6a_6z^5 + 8a_8z^7$. Finally, the experimental off-diagonal pressure tensor component P_{xz} needs to be fitted by an analytical curve. However, this is trivial, since the integrated density profile results in a linear relationship, i.e., P_{xz} can be fitted (Figure 2c) as $P_{xz}(z) = F_x\rho z$. Combining all these pieces of information, one arrives at $\eta(z) = -P_{xz}(z)/\gamma(z) = -F_x\rho/(2a_2 + 4a_4z^2 + 6a_6z^4 + 8a_8z^6)$.

In the second approach, the velocity profile is first smoothed and then the derivative of the smoothed velocity profile is determined numerically. The smoothing of the velocity profile prior to carrying out the derivate is essential, since the data are collected in narrow bins of about 0.05 Å, and thus, the scatter would result in huge oscillations of the shear rate if the smoothing was not applied. The viscosity profile is calculated as $\eta(z) = -P_{xz}(z)/\gamma(z)$. Since the numerically obtained curve of $\gamma(z)$ appears in the denominator of this formula, the resulting viscosity profile features diverging oscillations at points where $\gamma(z)$ changes sign, i.e., is close to zero. This happens close to the center of the slab, where the shear rate should be zero. As a result, this method is inaccurate at the center of the slab. However, with increasing distance from the center, i.e., when approaching the most interesting region, the accuracy increases. Even though it is not necessary and improves only the graphical presentation of the results around the center of the slab, we smoothed the numerically obtained shear $\gamma(z)$ prior to numerical determination of viscosity, shown in Figure 2d, to reduce the number of resulting oscillations of viscosity profile. The agreement between the curves obtained by analytical fit and by direct numerical derivative is excellent, apart from the center as explained. This further confirms that the results are insensitive to the choice of numerical procedure implemented (i.e., calculation of the derivative, smoothing). The oscillations in the shear rate numerically calculated from smoothed velocity profile, Figure 2b, in some regions might resemble a periodic pattern characteristic for a layered structure. However, these oscillations

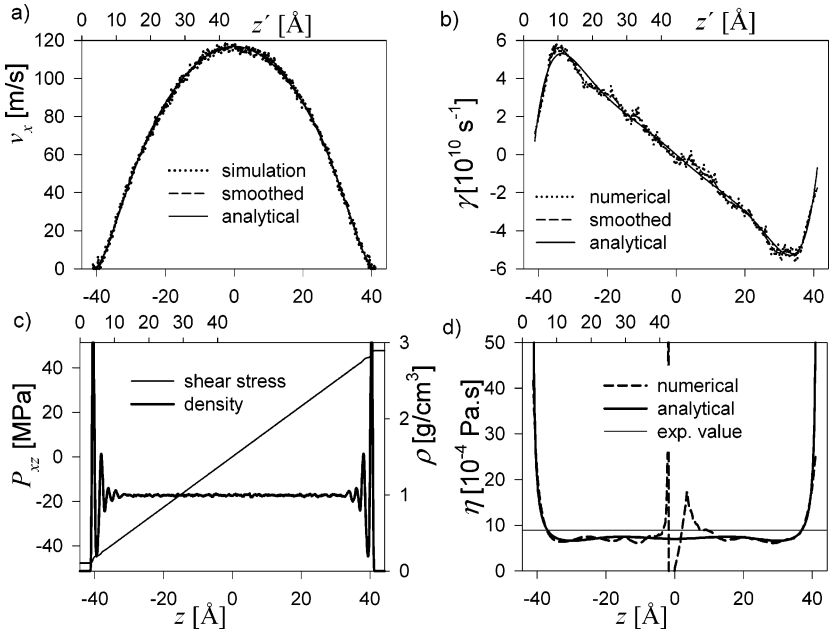

Figure 4. Same as in Figure 1, but for the wide slab.

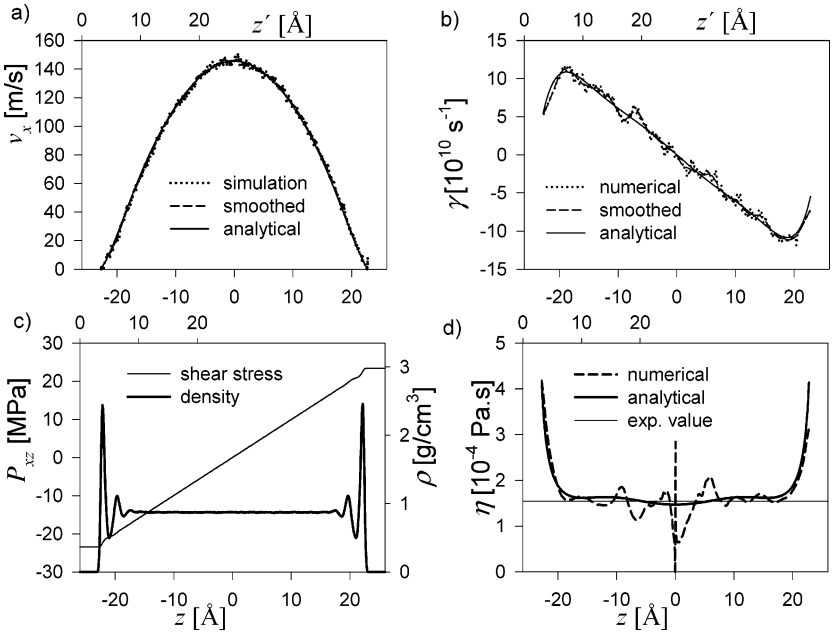

Figure 5. Velocity profile (a), shear rate (b), shear stress and density profile (c), and resulting viscosity profile (d) at 448 K and bulk density $\rho = 0.89$ g/cm^3, narrow slab. The experimental value of viscosity at 448 K is $\eta = 1.54 \times 10^{-4}$ Pa.s.[27]

are not symmetric with respect to the center of the slab, the spacing is not regular, and, first of all, no oscillations in the density or orientational alignment are observed at corresponding distances. Therefore, these oscillations are given by statistical inaccuracy of the numerical determination of the velocity gradient.

The resulting viscosity profile, shown in Figure 2d, reveals two distinct regions. At contact with the surface, viscosity reaches very high values, resulting from the adsorption of water molecules as discussed above. Although the inverse polynomial used to describe z-dependence of viscosity is not capable of predicting true divergence of $\eta(z)$ in the vicinity of the surface, the dependence reaches very high values at contact; that is, the polynomial fit of the velocity can predict even this behavior. The viscosity falls down to the bulk value sharply as the distance from the wall approaches about 10 Å. Further from the surface, at a distance of about 15 Å that can be identified as outer boundary of the interfacial layer, the bulk value is recovered, though the predicted value for SPC/E from our simulations is about 7.9×10^{-4} Pa.s, i.e., 11% below the experimental value 8.9×10^{-4} Pa.s for real water.[27,28] The results for the wide slab at ambient conditions (Figure 4), in all aspects, conform with those obtained in the narrow slab, particularly that the interfacial width is independent of the slab width. The same applied external force in both cases leads to about four times larger streaming velocity in the center of the wide slab, as expected. As a result, the streaming velocity in the center of the wide slab reaches about one-third of the root-mean-square velocity. However, the resulting viscosity profiles for the narrow and wide slabs perfectly agree.

Figures 5 and 6 give the results for high temperatures 448 and 523 K, respectively. With increasing temperature, the increase of viscosity at the contact layer becomes much smaller than at 298 K. The shear rate at short distances from the surface

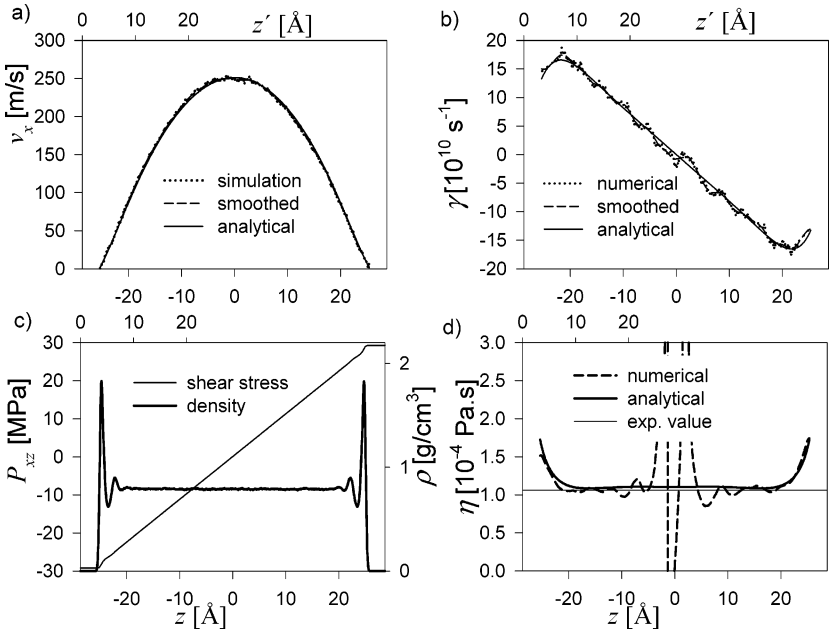

Figure 6. Velocity profile (a), shear rate (b), shear stress and density profile (c), and resulting viscosity profile (d) at 523 K and bulk density $\rho = 0.79$ g/cm^3, narrow slab. The experimental value of viscosity at 523 K is $\eta = 1.06 \times 10^{-4}$ Pa.s.[27]

remains nonzero, which leads to finite viscosity at contact, which reaches 280% and only 160% of corresponding bulk values at 448 and 523 K, respectively. This finding indicates that the water molecules in the second layer at these conditions are able to move along the surface, which is not the case at lower temperatures, as supported by the diffusivity profiles discussed bellow. At both high temperature states studied, the agreement of the viscosity in the bulk with experimental values is excellent, considering that the SPC/E model[13] was fitted to ambient conditions and was not fitted to dynamic properties at all.

Diffusivity. To further quantify the dynamics of water molecules and help in identifying the mobile and immobile layers, we also calculated the axial profile of lateral and perpendicular diffusivities D_{xy} and D_z, respectively. The method is described in detail in ref 1. The results presented here (i) use much narrower bins, which enables us to link directly the diffusivity profile with density and distance from the surface, (ii) include data for the wide slab, which provides evidence that our results do not depend on the surface separation, and (iii) include the data for 523 K not studied before. For this goal, we used equilibrium molecular dynamics simulations and a standard Nosé thermostat acting on all translational and rotational velocities.

The diffusivities are calculated from the slope of the mean square displacement (MSD) of water molecules as a function of time. In contrast to ref 1, we divide the slab into 200 bins that, after averaging over the two surfaces, leads to 100 bins covering distances $0-L_z/2$ from the surface. The resulting bin width is therefore about 0.3 Å for the narrow slab and 0.5 Å for the wide slab. The typical development of the MSD in selected bins is shown in Figure 7. To localize the molecule in terms of initial and final positions defining the MSD (when these two bins differ, half of the MSD is ascribed to each of the two bins), the MSD is tracked for time intervals up to 2.4 ps only and the slope is determined from the linear regime between 1.2 and 2.4 ps. Rough estimate of the displacement of a molecule within 2.4 ps, $\Delta z = (2Dt)^{1/2}$, substituting the bulk diffusivity 2.7×10^{-9} m^2/s leads to 1.1 Å, which means that an individual molecule can diffuse to neighboring bins, but is well localized.

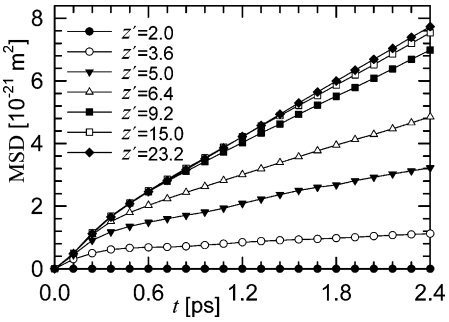

Figure 7. Average mean square displacement of water molecules in the direction perpendicular to surface as a function of their distance z' from a surface at ambient conditions in a narrow slab. The plot for direction parallel with the surface looks qualitatively the same.

From the slopes of MSD in each of the 100 bins, the diffusivity profile shown in Figure 8 was constructed. The top graph, showing the data for 298 K, confirms that enlarging the slab width has no effect on the interfacial region, and in both cases, the bulk-like diffusivity of both components is obtained at about 15 Å. The bulk diffusivity[28] of SPC/E, 2.7×10^{-9} m^2/s, is accurately reached by the perpendicular diffusivity; the value of parallel diffusivity is about 10% higher. The experimental value of real water diffusivity at 300 K, also indicated in Figure 8, is only 2.3×10^{-9} m^2/s,[29,30] i.e., significantly lower. The diffusivity profile correlates with the density profile; namely, we observe a shoulder of diffusivity around 5 Å in the region of low density between the second and third layer of water molecules. The peak of diffusivity at 3 Å corresponds to penetration of a few molecules to a region of practically zero density and is of little importance.

The high-temperature data, shown in the bottom part of Figure 8, reveals a qualitatively similar behavior to that at ambient conditions. However, the diffusivity in the second layer of water molecules (~3.7 Å), which is only about 10% of the bulk value at 298 K, increases to 20% of the bulk value at 448 and nearly 50% at 523 K. The diffusivity in the third layer (~6 Å) is approximately 50% of the bulk value at all temperatures. The parallel diffusivity in all cases approaches the bulk diffusivity

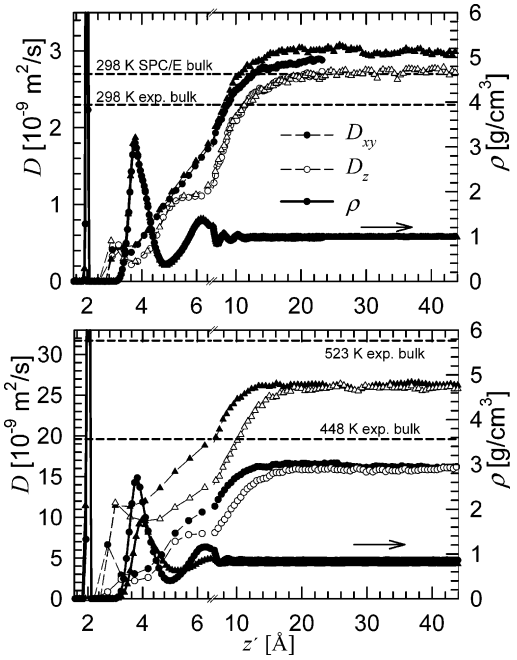

Figure 8. Perpendicular (open symbols) and parallel (filled symbols) diffusivity as a function of distance z' from the surface. The experimental bulk diffusivities are given by dashed lines. The density profile of water is given by solid line with a corresponding symbol and right vertical axis. Top: 298 K, narrow slab (circles) and wide slab (triangles). Bottom: wide slab, 448 K (circles) and 523 K (triangles). The scale of the horizontal axes for distances smaller than 6.5 Å is expanded for clarity.

faster than the perpendicular component, which is characteristic for a layered structure. The observed bulk diffusivity of SPC/E at 448 K, 16.0×10^{-9} m^2/s, is lower than the experimental value 19.6×10^{-9} m^2/s.[31] The observed bulk diffusivity of SPC/E at 523 K, 26.0×10^{-9} m^2/s, is also definitely lower than the experimental value, though only the extrapolated data[30] 31.7×10^{-9} m^2/s is used for comparison in this case.

6. Conclusions

We have demonstrated the local viscosity variation of a molecular fluid, namely SPC/E water, in contact with the atomically detailed rutile (110)[1,2] surface using molecular simulations. In contrast to previous viscosity determination, which was applied to a simple surface composed by charged LJ atoms arranged in a square lattice,[11] we used atomically detailed rutile surface based on ab initio relaxed surface with flexible surface O and H atoms within ab initio obtained bond lengths and potentials.

The method is based on a simple equation linking the off-diagonal pressure tensor component P_{xz} to the easily accessible axial density profile of water molecules. Using this method, we were able to obtain dependence of local viscosity of water on distance from the surface. In all cases, the velocity profile is monotonically increasing with distance from the surface, and therefore, the local viscosity is well-defined at all points, as opposed to some studies of atomic systems[6,10] and SPC/E water in silicon nanochannels,[12] which reported decreasing velocity profiles in certain regions, leading to negative values of local viscosity at those regions. The determination of the inhomogeneous diffusivities of water molecules, with a spatial resolution less than 0.5 Å, was found to be very accurate, mostly due to the long simulation run compared to the time over which the mean square displacement needs to be tracked.

The first layer of water molecules at 2−2.3 Å, chemisorbed at hydroxylated surface and physisorbed at the nonhydroxylated surface, is completely immobile at all temperatures, as proved by zero diffusivity and zero streaming velocity of this layer. The second layer of water molecules at 3.7 Å becomes increasingly mobile with increasing temperature. At 298 K the diffusivity and the streaming velocity in the applied field are small in this layer, which leads to the steep rise of the viscosity at contact with rutile surface. At 448 and 523 K the second layer becomes more mobile, and the viscosity in this layer is only 180%, respectively 60% higher than in the corresponding bulk.

We found earlier that the structural properties of both water and dissolved ions become bulklike at distances larger than 15 Å.[1,2,5] Current results indicate that not only the structural but also the dynamic properties, represented here by shear viscosity and diffusivity, become bulklike at such a short distance from the surface. The interfacial width remains unchanged even in the presence of flow introduced by applied external force. This finding is in contrast with the location of the shear plane obtained from simplified models of the electric double layer using as input zeta potential calculated from the Helmholtz−Smoluchowski equation, which combines experimentally determined mobility with assumed bulklike viscosity and permittivity of solution. We were able, by determining the viscosity and diffusivity profiles at the interface, not only to specify the interfacial width, but also to test the assumption of constant, bulk-like viscosity, which is implicit in the Helmholtz−Smoluchowski equation. The viscosity profile is rather flat, outside of its steep rise in contact with the surface, and cannot be fully responsible for the discrepancies between our findings and the location of shear plane predicted by the interpretation of the electrophoretic data. Similar discrepancies have been noted by others[32−34] and have been attributed to various deficiencies in the Helmholz−Smoluchowski equation including its neglect of surface curvature, surface conduction in both immobile and diffuse layers, and polarization of the EDL. Consequently, the determination of the dielectric properties of the interface is a logical next step to further understanding of the complex properties of metal-oxide/aqueous solution interface.

As a byproduct, we found an excellent agreement between the experimental values of viscosity of real water with our predictions using the SPC/E model of water at liquid densities and temperatures up to 523 K. On the contrary, SPC/E overpredicts the bulk diffusivity at 298 K and underpredicts experimental values at high temperatures.

Acknowledgment. This research was supported by the Grant agency of the Czech Republic (Grant No. 203/03/P083), by the National Research Program "Information Society" (Project No. 1ET400720507), and by the Division of Chemical Sciences, Geoscience and Biosciences, Office of Basic Energy Sciences, U.S. Department of Energy under Contract DE-AC05-00OR22727, Oak Ridge National Laboratory, managed and operated by UT−Battelle, LLC. The authors wish to thank Michael L. Machesky, Jerome Delhommelle, and Billy Todd for stimulating discussions and provision of manuscript prior to publication.

References and Notes

(1) Předota, M.; Bandura, A. V.; Cummings, P. T.; Kubicki, J. D.; Wesolowski, D. J.; Chialvo, A. A.; Machesky, M. L. *J. Phys. Chem. B* **2004**, *108*, 12049.

(2) Předota, M.; Cummings, P. T.; Zhang, Z.; Fenter, P.; Wesolowski, D. J. *J. Phys. Chem. B* **2004**, *108*, 12061.

(3) A comment on refs 1 and 2 to correct errors introduced by an error in the calculation of one of the terms of surface−solution force can be found here: Předota, M.; Vlcek, L. *J. Phys. Chem. B* **2007**, *111*, 1245.

(4) Zhang, Z.; Fenter, P.; Cheng, L.; Sturchio, N. C.; Bedzyk, M. J.; Machesky, M. L.; Wesolowski, D. J. *Surf. Sci.* **2004**, *554*, L95.

(5) Zhang, Z.; Fenter, P.; Cheng, L.; Sturchio, N. C.; Bedzyk, M. J.; Předota, M.; Bandura, A.; Kubicki, J.; Lvov, S. N.; Cummings, P. T.; Chialvo, A. A.; Ridley, M. K.; Bénézeth, P.; Anovitz, L.; Palmer, D. A.; Machesky, M. L.; Wesolowski, D. J. *Langmuir* **2004**, *20*, 4954.

(6) Travis, K. P.; Gubbins, K. E. *J. Chem. Phys.* **2000**, *112*, 1984.

(7) Zhang, J.; Todd, B.D.; Travis, K. P. *J Chem. Phys.* **2004**, *121*, 10778.

(8) Delhommelle, J. *Phys. Rev. E* **2005**, *71*, 016705.

(9) Zhu, W.; Singer, S. J.; Zheng, Z.; Conlisk, A. T. *Phys. Rev. E* **2005**, *71*, 041501.

(10) Thompson, A. P. *J. Chem. Phys.* **2003**, *119*, 7503.

(11) Freund, J. B. *J. Chem. Phys.* **2002**, *116*, 2194.

(12) Qiao, R.; Aluru, N. R *J. Chem. Phys.* **2003**, *118*, 4692.

(13) Berendsen, H. J. C.; Grigera, J. R.; Straatsma, T. P. *J. Phys. Chem.* **1987**, *91*, 6269.

(14) Bandura, A. V.; Kubicki, J. D. *J. Phys. Chem. B* **2003**, *107*, 11072.

(15) Bandura, A. V.; Sykes, D. G.; Shapovalov, V.; Troung, T. N.; Kubicki, J. D.; Evarestov, R. A. *J. Phys. Chem. B* **2004**, *108*, 7884.

(16) Fedkin, M. V.; Zhou, X. Y.; Kubicki, J. D.; Bandura, A. V.; Lvov, S. N. *Langmuir* **2003**, *19*, 3797.

(17) Delgado, A. V.; Gonzalez-Caballero, E.; Hunter, R. J.; Koopal, L. K.; Lyklema, J. *Pure Appl. Chem.* **2005**, *77*, 1753.

(18) Brown, G. E., Jr.; et al. *Chem. Rev.* **1999**, *77*, 99.

(19) Kallay, N.; Čop, A.; Kovačevic, D.; Pohlmeier, A. *Progr. Colloid Polym. Sci.* **1998**, *109*, 221.

(20) Allen, M. P.; Tildesley, D. J. *The Computer Simulation of Liquids*; Clarendon Press: Oxford, 1987.

(21) Frenkel, D.; Smit, B. *Understanding Molecular Simulations: From Algorithms to Applications*; Academic Press: San Diego, 1996.

(22) Mondello, M.; Grest, G. S. *J. Chem. Phys.* **1997**, *106*, 9327.

(23) Bedrov, D.; Smith, G. D.; Sewell, T. D. *J. Chem. Phys.* **2000**, *112*, 7203.

(24) Travis, K. P.; Todd, B. D.; Evans, D. J. *Phys. Rev. E* **1997**, *55*, 4288.

(25) Todd, B.D.; Evans, D. J. *Phys. Rev. E* **1996**, *55*, 2800.

(26) Delhommelle, *J. Phys. Rev. B* **2004**, *69*, 144117.

(27) Lemmon, E. W.; McLinden, M. O.; Friend, D. G. "Thermophysical Properties of Fluid Systems" in NIST Chemistry WebBook, NIST Standard Reference Database Number 69; Linstrom, P. J., Mallard, W. G., Eds; National Institute of Standards and Technology: Gaithersburg MD, 2005; http://webbook.nist.gov.

(28) Smith, P. E.; van Gunsteren, W. F. *Chem. Phys. Lett.* **1993**, *215*, 315.

(29) Lamanna, R.; Delmelle, M.; Cannistraro, S. *Phys. Rev. E* **1994**, *49*, 2841.

(30) Mills, R. *J. Phys. Chem.* **1973**, *77*, 685.

(31) Krynicki, K.; Green, C. D.; Sawyer, D. W. *Faraday Discuss. Chem. Soc.* **1978**, *66*, 199.

(32) Lyklema, J. *Fundamentals of Interface and Colloidal Science. Vol. II-Solid-Liquid Interfaces*; Academic Press: San Diego, 1995.

(33) Lyklema, J.; Rovillard, S.; De Coninck, J. *Langmuir* **1998**, *14*, 5659.

(34) Hunter, R. J. *Foundations of Colloidal Science*; Oxford University Press: Oxford, 2001.